A Study on the Preparation of Konjac Glucomannan-silk Fibroin Composite Aerogels and Its Adsorption of Water Pollutant Cr(Ⅲ)①

CHEN Han[a, e] WU Chun-Hua[a, b, c, d②]
HUANG Yi[e] WU Hua-Hua[e] PANG Jie[a, b, c, d②]
[a] (*Engineering Research Centre of Fujian-Taiwan Special Marine Food Processing and Nutrition, Ministry of Education, Fuzhou* 350002, *China*)
[b] (*State Key Laboratory of Food Safety Technology for Meat Products, Xiamen* 361100, *China*)
[c] (*College of Food Science, Fujian Agriculture and Forestry University, Fuzhou* 350002, *China*)
[d] (*Key Laboratory of Marine Biotechnology of Fujian Province, Institute of Oceanology, Fujian Agriculture and Forestry University, Fuzhou* 350002, *China*)
[e] (*Fujian University of Technology, Fuzhou* 350118, *China*)

ABSTRACT It is emergent to develop a green waste water adsorbent with high efficiency. Therefore, a type of low-cost, green and environmentally friendly konjac glucomannan (KGM) -silk fibroin (SF) composite aerogels were compounded via simple chemical grafting and vacuum freeze drying, and a study on its adsorption capacity was also conducted. The characterizations of FT-IR, SEM, XRD and DSC indicate that the modified aerogels show a porous network space structure and there is a strong hydrogen bond effect between the KGM and SF molecules, which improves the density, compressive strength and thermal stability of aerogel materials. The adsorption experiments show that KGM-SF aerogels can effectively adsorb the water pollutants Cr(Ⅲ) with a maximal adsorption capacity of 82 mg g^{-1}. In addition, the adsorption isotherm and dynamic model analysis are used to elaborate the adsorption mechanism of KGM-SF aerogels and explain that the composite aerogels can be single molecule chemisorption. KGM-SF aerogels have potential adsorption capacity.

Keywords: konjac glucomannan, silk fibroin, aerogel, adsorption, Cr(Ⅲ)
DOI: 10.14102/j.cnki.0254–5861.2011–2774

1 INTRODUCTION

With the advancement of industrialization, heavy metal pollution in oceans and other water is becoming increasingly serious, and its teratogenicity and carcinogenicity are threatening on human health and have attracted great concern[1-4]. As a method for the separation and disposal of heavy metals, the adsorption method has arose great concern and research due to its advantages of simple operation, technical maturity and wide application[5, 6] .

Aerogels are a kind of advanced materials with promising applications in chemical engineering, biomedical, food and pharmacetical area[7, 8] . Recent researches discover that aerogel materials as the carrier for immobilization have good adsorption effects[9-13]. However, the recycling[14] and degradation[15] after adsorption are another difficult process and also cause recontamination, which to great extent restricts its application. Therefore, producing a natural, degradable and high-performance aerogel material has become one of the research hotspots in the polymer material field[16-22].

KGM, a natural polysaccharide polymer with excellent biocompatibility, biodegradability, and hydrophilicity has been used in materials, food, and biomedical fields[23-27]. Taking the water pollutant Cr(Ⅲ) as an example, this research used SF to modify KGM, prepared KGM-SF aerogels, characterized its structure by the use of fourier infrared spectrometer (FT-IR), scanning electron microscope (SEM), X-ray diffractometer (XRD) and differential scanning calo-

Received 21 February 2020; accepted 16 March 2020
① This work was financially supported by the National Natural Science Foundation of China (31471704, 31772045)
② Corresponding authors. E-mails: chwu0283@163.com and pang3721941@163.com

rilmeter (DSC), and researched its strength and thermal stability. Meanwhile, the effects of the dosage of KGM-SF aerogels adsorbent, contact time, the pH of the solution and initial concentration on adsorbing Cr(Ⅲ) were investigated so as to provide a theoretical basis and guide for the development and application of aerogels made of natural polymer polysaccharide in the field of immobilization carrier materials.

2 EXPERIMENTAL

2. 1 Materials

Konjac glucomannan (KGM) (purity ⩾ 95%, viscosity: 1.5% solution, ⩾ 35,000 MPas) was purchased from Yizhi Konjac biological technology Co. Ltd. (Hubei, China). Silk fibroin (SF) (average molecule weight (Mw): 90) was provided by Huzhou Xintiansi Bio-tech Co., Ltd. (Zhejiang, China). The adsorbates (Cr(Ⅲ)) used in this study were supplied by Shanghai Macklin Biochemical Technology Co., Ltd. (Shanghai, China). All other reagents (analytical grade) were purchased from Sinopharm Chemical Reagent Co., Ltd. (Shanghai, China). Purified water with a resistance greater than 18 MΩ·cm^{-1} was used in all experiments.

2. 2 Preparation of KGM aerogels

The quantitative KGM was placed at normal temperature and dispersed in 100 mL deionized water under a 350 rpm stirring for 60 mins. Then a KGM sol solution of 3% (w/v, w in gram and v in milliliter) was obtained and stored in a 4 ℃ refrigerator for 24 h. The KGM aerogels were then obtained after 18 h of liquid nitrogen quick freezing and vacuum freeze drying.

2. 3 Preparation of KGM-SF aerogels

KGM-SF aerogels synthesized by adopting a sol-gel method under freeze-drying are shown in Fig. 1. The SF solution was obtained through dissolving 300 mg SF in 10 mL deionized water[28]. The SF solution and KGM sol solution at a ratio of 1:1 were stirred with a rotation speed of 350 rpm in a constant temperature water bath for 60 mins and stored in a 4 ℃ refrigerator for 24 h. Finally, KGM-SF aerogels were obtained after 18 h of liquid nitrogen quick freezing and vacuum freeze drying.

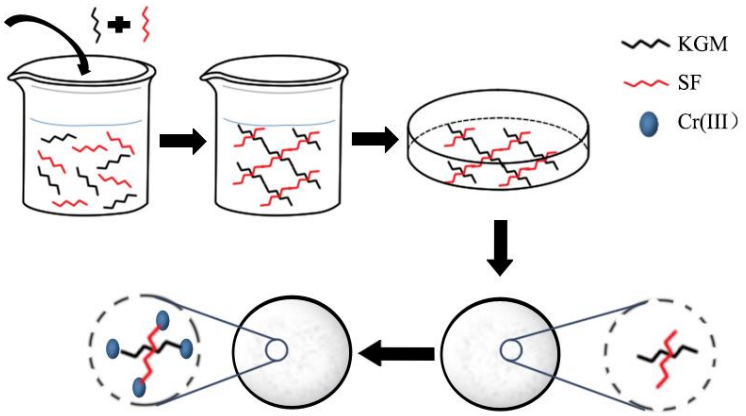

Fig. 1. Conceptual graph of KGM-SF aerogels preparation and adsorption

2. 4 Characterization of aerogels

The Fourier transform infrared spectra of the aerogels were performed by using a Nicolet 6700 FTIR spectrometer (FT-IR, Nicolet 6700, Thermo Fisher Scientific Co., Ltd., USA) in the range of 4000～500 cm^{-1}. The structural morphology of the aerogels was determined using scanning electron microscopy (SEM, Hitachi S-4800, Hitachi, Japan). The phase structures of KGM/SF aerogels were investigated through X-ray diffraction on a D8 Advance XRD diffractometer (XRD, Bruker AXS D8 Advance, Bruker Inc., Germany) with Cu-NF filter at a scan rate of 0.1/s. DSC was measured with a DSC200F3 instrument (Zetzsch, Germany) from 25 to 150 ℃ at a rate of 5 ℃·min^{-1} under nitrogen flow at a rate of 50 mL·min^{-1}.

2. 5 Adsorption test of Cr(Ⅲ) by KGM-SF aerogels

Approximately, 15 mg KGM-SF aerogels was added to the conical flask containing 25 mL Cr(Ⅲ) solution, and its pH was adjusted by adding $HClO_4$ and NaOH solutions. Then it was placed in a constant temperature water bath shaker and shaken for a certain time. The concentration of Cr(Ⅲ) before and after adsorption in the solution was measured by using ICP-OES in the Ultraviolet and Visible Spectrophotometry (n = 652 nm)[29, 30]. All the experiments were performed twice to get the average results.

The equilibrium adsorption capacity (q_e/mg g^{-1}), partition coefficient (K_d/ml g^{-1}), and the adsorption rate (S) of KGM-SF aerogels for Cr(Ⅲ) were calculated respectively via the equations (1～3).

$$q_e = \frac{(C_0 - C_e)\times V}{m} \quad (1)$$

$$W_d = \frac{(C_0 - C_e)\times V}{C_0 \times m} \quad (2)$$

$$S = \frac{C_0 - C_e}{C_0} \times 100\% \quad (3)$$

In the above equations, C_0 represents the initial concentration of the metal ions, C_e is the equilibrium concentration of the metal ions, V means the volume of the solution measured, and m stands for the mass of the adsorbent.

3 RESULTS AND DISCUSSION

3. 1 FT-IR, SEM, XRD, and DSC analyses

The FT-IR spectra of KGM and KGM-SF aerogels in the range from 4000 to 500 cm^{-1} are shown in Fig. 2. The peaks between 3000 and 2800 cm^{-1} are the C–H stretching vibration of CH_2 group and C–H of CH_3 in the saturated structure, and the absorption peak intensity of KGM-SF aerogels within the range of 1500～1350 cm^{-1} becomes stronger, which explains that Maillard reaction can lead to the increase of C–OH vibration and C–H deformation vibration[31-34], and these two groups of peaks also verify the existence of carbohydrate in KGM aerogels. Amide Ⅱ band can vividly display the hydrogen-bond interaction between or in macromolecules[35, 36]. Compared with KGM aerogels, the peak intensities of KGM-SF aerogels in the amide I band (1700～1600 cm^{-1}) and amide II band (1600～1500 cm^{-1}) show an increasing trend, and the corresponding absorption peaks also shift toward high wave numbers. In Fig. 2, the changes of the peak shape of the amide I band in KGM-SF aerogels further explain that the SF intramolecular structure is destroyed; in the KGM-SF aerogels, an absorption peak disappearing in the KGM aerogels appears in the amide II band, which indicates the presence of strong hydrogen bonding between protein and polysaccharide molecules after the covalent bonding of KGM and SF (Fig. 3).

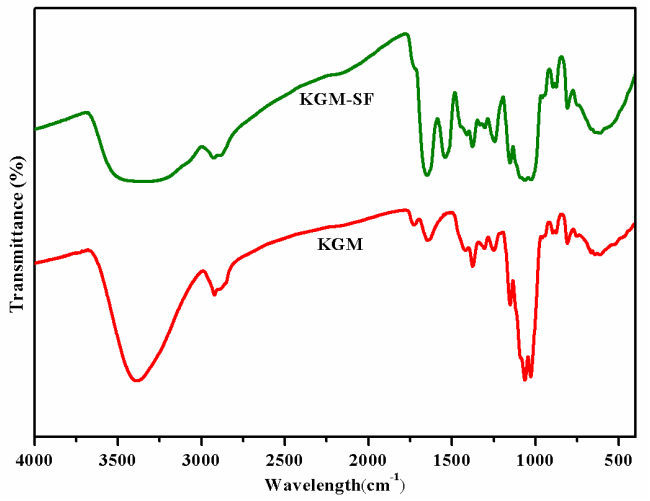

Fig. 2. FT-IR spectra of KGM and KGM-SF

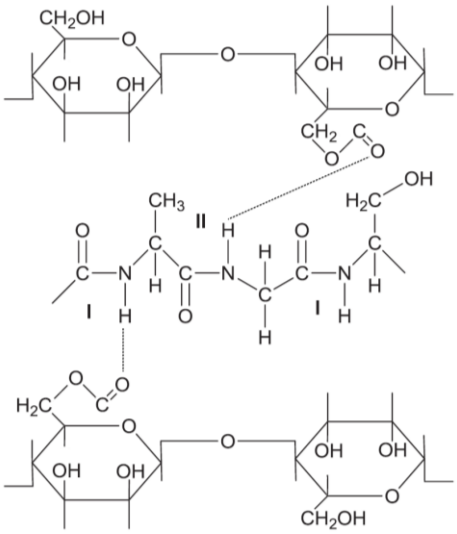

Fig. 3. Hydrogen bonds between KGM and SF

As shown in Fig. 4(a) and 4(b), both KGM and KGM-SF aerogels show white sponge-like shape when observed with the naked eyes. Using SEM to observe its microstructure, it can be seen from the figure that compared with KGM aerogels, the hydrogen bonding between KGM and SF in KGM-SF aerogels forms a dense and ordered porous network cross-linked structure, indicating that SF can improve the stability of KGM aerogels; the interaction between KGM and SF reduces the aggregation of KGM molecules, further reduces the pore sizes of aerogels, increases the surface area, and enhances the interaction between molecules. Therefore, these regular porous network structure pores can provide more metal adsorption sites, which is conducive to obtaining nano porous network adsorption materials with ideal adsorption capacity[37, 38]. This may be due to the strong hydrogen bonding interaction between SF and the functional groups.

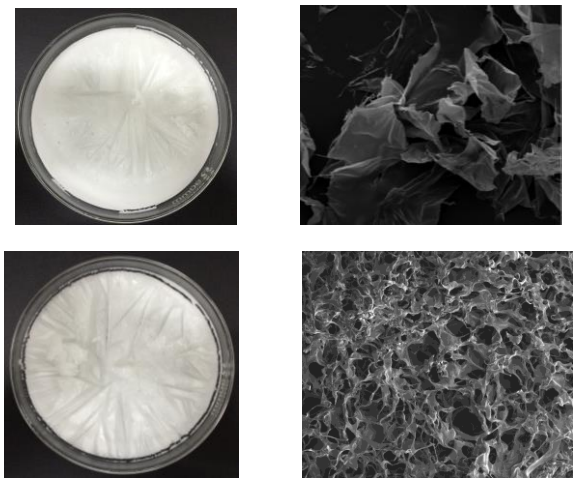

Fig. 4. Photographs of (a) KGM and (b) KGM-SF; SEM images of (c) KGM and (d) KGM-SF

It can be seen from Fig. 5(a) that KGM aerogels have no significant crystallization peak within the whole scanned area and shows an undefined structure, and there is only a wide diffuse peak at 2θ = 20.14 º. From the diffraction spectrum of KGM-SF aerogels, it can be discovered that the diffuse peak of KGM aerogels is strengthened due to the addition of SF. This shows a strong interaction between KGM and SF. Through cross-linking, intramolecular and intermolecular hydrogen bonding, KGM and SF make the molecular chains intertwined, thus forming a stable porous network structure, and can serve as a physical cross-linking point to increase the cross-linking density of aerogel materials, so that the density and compressive strength of aerogels can be improved[39]. It also proves a good compatibility between KGM and SF.

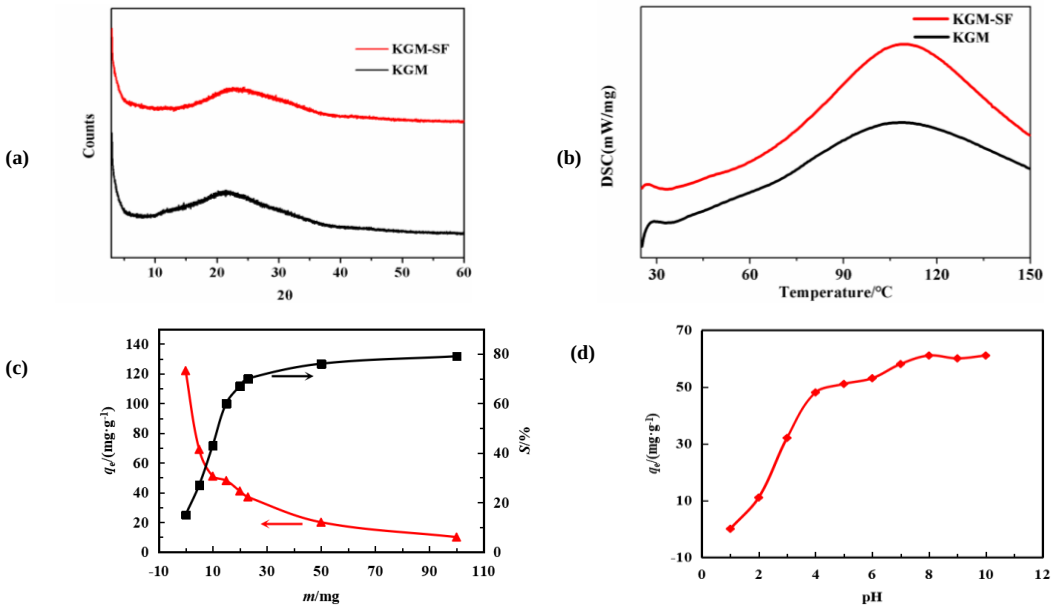

Fig. 5. (a) XRD patterns of KGM and KGM-SF; (b) DSC patterns of KGM and KGM-SF; (c) Effect of sample volumes on the adsorption capacity (*qe*) of Cr(Ⅲ); (d) Effect of pH on the adsorption capacity of Cr(Ⅲ)

It can be seen that both KGM and KGM-SF aerogels exhibit two main thermal transition peaks from Fig. 5(b). The Td of the KGM-SF aerogel sample is 99.0 ℃ and the Ti is 31.6 ℃, while those of the KGM aerogels sample are 117.2 and 29.1 ℃, respectively. Compared with KGM aerogels, the endothermic peaks of KGM-SF aerogels are sharper and narrower, which indicates that the latter are more stable. In terms of enthalpy (ΔH), 0.2226 J/g of KGM-SF aerogels is higher than that of KGM aerogels, which explains the SF can improve the thermal stability of KGM aerogels[40].

3. 2 Effect of the amount of adsorbent on adsorption

As shown in Fig. 5(c), with the increase of sample amount, the adsorption capacity of KGM-SF aerogels to Cr(Ⅲ) decreases, but the adsorption rate increases. When the 15 mg sample was added, the adsorption capacity of KGM-SF aerogels to Cr(Ⅲ) exceeded 50 mg g^{-1}, and the adsorption rate of KGM-SF aerogels to Cr(Ⅲ) could reach about 62%. Since the sample amount needed under this condition was small and the better adsorption effect could be achieved, all subsequent experiments chose 15 mg KGM-SF aerogels as the amount of adsorbent at the optimal point.

3. 3 Effect of pH on the adsorption

Fig. 5(d) represents the effect of pH on the adsorption capacity of KGM-SF aerogels to Cr(Ⅲ). In water solution, the pH value significantly affects the binding sites, surface charge and existence form of Cr(Ⅲ), thus becoming an important parameter of affecting the adsorption capacity of Cr(Ⅲ). From Fig. 5(d), it can be seen that when the pH of the solution is 1.0～4.0, the growth rate of the adsorption capacity of the sample is the fastest; it gradually slows down when the pH value is 4.0～8.0; and it finally stabilizes at the pH of 8.0～10.0. The reason for this phenomenon is that when pH < 4.0, H^+ in the solution competes with the adsorption sites on the KGM-SF aerogels; when 4.0<pH<8.0, the adsorption capacity of KGM-SF aerogels increases due to the electrostatic attraction in the system; when pH > 8.0, the adsorption capacity of KGM-SF aerogels increases because of the precipitation in the system.

3. 4 Analysis of adsorption isotherm

The effect of different initial concentrations on the KGM-SF aerogels' adsorption capacity of Cr(Ⅲ) is shown in Fig. 6(a), in which the KGM-SF aerogels' adsorption capacity of Cr(Ⅲ) displays a growing trend with increasing the initial concentration of Cr(Ⅲ). When the initial concentration of Cr(Ⅲ) reaches 200 mg L^{-1}, the adsorption capacity of the sample is about 82 mg g^{-1}. Researches on the adsorption isotherm are also made to further understand the functional mechanism of the interaction between the adsorbent substances and the adsorbent solvents[41, 42]. This process describes the relationship between the concentration of adsorbent and the adsorption capacity through two isothermal adsorption model equations: Freundlich isotherm and Langmuir isotherm[43]. The equation linear representations of Langmuir and Freundlich are respectively shown in equations (4) and (5). From the results of Fig. 6(b) and 6(c), the assumed Langrnuir model based on the single molecule adsorption has a higher fitting correlation coefficient compared with the correlation coefficient of the Freundlich model. Therefore, the KGM-SF aerogels' adsorption of Cr(Ⅲ) may be a process of single molecular adsorption.

$$\frac{C_e}{q_e} = \frac{1}{bq_m} + \frac{C_e}{q_m} \tag{4}$$

$$\ln q_e = \ln K_F + \frac{1}{n}\ln C_e \tag{5}$$

In the above equations, b is the equilibrium constant, q_m is the maximal adsorption capacity of Langmuir monolayer adsorption, and K_F and n represent the empirical coefficients in the process of adsorption within a certain range.

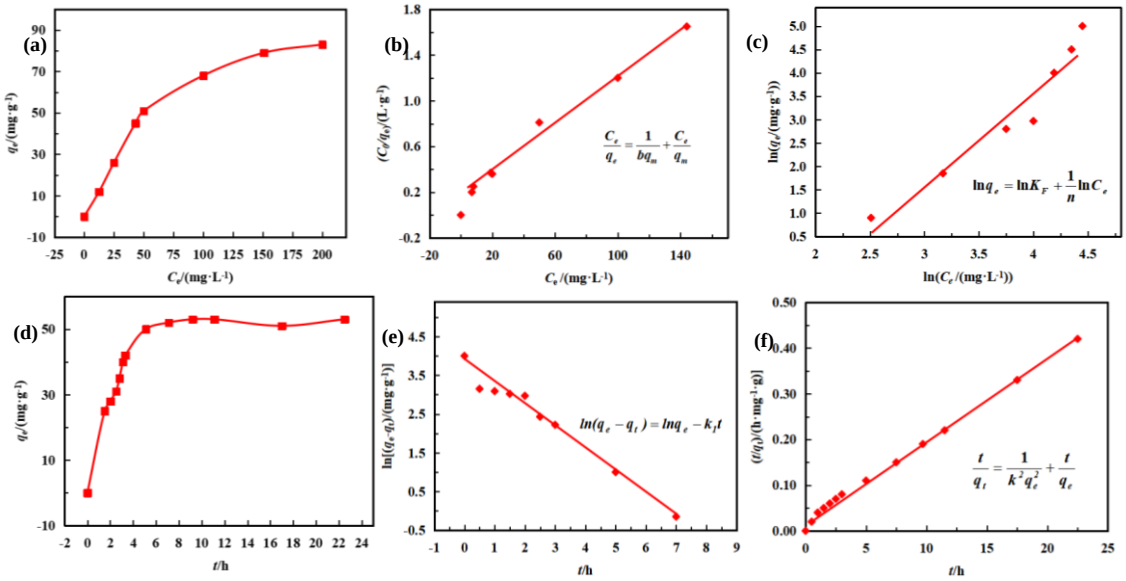

Fig. 6. (a) Effect of the initial concentration on adsorption capacity of Cr(Ⅲ); (b) Langmuir isotherm model; (c) Freundlich isotherm model; (d) Effect of contact time on the adsorption capacity of Cr(Ⅲ); (e) Pseudo-first order kinetic model; (f) Pseudo-second order kinetic model

3. 5 Analysis of the adsorption kinetics

Fig. 6(d) represents the effect of time on the adsorption capacity of KGM-SF aerogels. It can be seen that the growth rate of adsorption capacity is rapid in a few hours of the initial contact, reaching about 65% of the equilibrium adsorption capacity, and the adsorption reached equilibrium at about 10 h. The pseudo-first and pseudo-second order kinetic models can be applied to the researching process of adsorption[44]. The two models are respectively represented by equations (6) and (7).

$$\ln(q_e - q_t) = \ln q_e - k_1 t \tag{6}$$

$$\frac{t}{q_t} = \frac{1}{k_2 q_e^2} + \frac{t}{q_e} \tag{7}$$

In the above equations, q_e stands for the adsorption capacity at the equilibrium state, q_t represents the adsorption capacity at any time (t), and k_1 and k_2 are the adsorption rate constants of the pseudo-first and pseudo-second order kinetics, respectively. Fig. 6(e) shows the pseudo-first order kinetic model, and Fig. 6(f) represents the pseudo-second kinetic model. Though making an analysis and comparison, the pseudo-second order kinetic model based on chemical adsorption is found to be more suitable to describe the process of KGM-SF aerogels adsorption of Cr(Ⅲ). Therefore, KGM-SF aerogels adsorption of Cr(Ⅲ) is mainly a chemical adsorption process. The KGM-SF aerogels prepared in this study are a perfect support that can hold the micro particles to perform the adsorption ability. The obtained KGM-SF aerogels constitute a feasible option as a Cr(Ⅲ) sorbent due to its potentially low cost and environmentally benign nature.

4 CONCLUSION

In conclusion, this research has developed KGM-SF aerogels with a porous network structure, which endows it with high order, high strength, stable thermal properties and more unique mechanical performance. The results of FT-IR, SEM, XRD and DSC spectra indicate that there is good compatibility between KGM and SF, and there is a strong hydrogen bond between KGM and SF molecules in KGM-SF aerogels, which may be the main reasons for the improvement of its performance; the adsorption results indicate that KGM-SF aerogels can stably exist in the water solution and have certain adsorption effects on the water pollutant Cr(Ⅲ). Its maximal adsorption capacity is about 82 mg g^{-1}, and the equilibrium time is about 10 h, which also verifies that the pH of the adsorbent has a significant effect on the adsorption capacity; the experimental results show that the Langmuir isothermal model and pseudo-second order kinetic model are more suitable to describe KGM-SF aerogels' adsorption process of the water pollutant Cr(Ⅲ), and that the process may be single molecule chemisorption.

REFERENCES

(1) Yang, Y.; Zhou, Z. C.; Bai,Y. Y.; Cai, Y. M.; Chen,W. P. Risk assessment of heavy metal pollution in sediments of the fenghe river by the fuzzy synthetic evaluation model and multivariate statistical methods. *Pedosphere* **2016**, 26, 326–334.

(2) Ratnakar, S.; Bhabagrahi, S. Mapping of heavy metal pollution in river water at daily time-scale using spatio-temporal fusion of MODIS-aqua and Landsat satellite imageries. *J. Environ. Manage.* **2017**, 192, 1–14.

(3) Sarma, G. K.; Sen Gupta, S.; Bhattacharyya, K. G. Nanomaterials as versatile adsorbents for heavy metal ions in water: a review. *Environ. Sci. Pollut. R.* **2019**, 26, 6245–6278.

(4) Chu, Z. J.; Fan, X. H.; Wang, W. N.; Huang, W. C. Quantitative evaluation of heavy metals' pollution hazards and estimation of heavy metals' environmental costs in leachate during food waste composting. *Waste Manage.* **2019**, 84, 119–128.

(5) Ihsanullaha; Aamir, A.; Adnan, M. A.; Tahar, L.; Mohammed, J. A. M.; Mustafa, S. N.; Majeda, K.; Muataz, A. A. Heavy metal removal from aqueous solution by advanced carbon nanotubes. *Sep. Purif. Technol.* **2016**, 157, 141–161.

(6) Burakov, A. E.; Galunin, E. V.; Burakova, I. V.; Kucherova, A. E.; Agarwal, S.; Tkachev, A. G.; Gupta, V. K. Adsorption of heavy metals on conventional and nanostructured materials for wastewater treatment purposes. *Ecotox. Environ. Safe.* **2017**, 148, 702–712.

(7) Chen, K. L.; Zhang, H. Alginate/pectin aerogel microspheres for controlled release of proanthocyanidins. *Int. J. Biol. Macromol.* **2019**, 136, 936–943.

(8) Chen, K. L.; Zhang, H. Fabrication of oleogels via a facile method by oil absorption in the aerogel templates of protein-polysaccharide conjugates. *ACS Appl. Mater. Inter.* **2020**, 12, 7795–7804.

(9) Borsagli, M.; Fernanda, G. L.; Mansur, A. A. P.; Poliane, C.; Oliveira, L. C. A.; Mansur, H. S. O-carboxymethyl functionalization of chitosan: complexation and adsorption of Cd(II) and Cr(VI) as heavy metal pollutant ions. *React. Funct. Polym.* **2015**, 97, 37–47.

(10) Kim, K. H.; Oh, Y.; Islam, M. F. Graphene coating makes carbon nanotube aerogels superelastic and resistant to fatigue. *Nat. Nanotechnol.* **2012**, 7, 562–566.

(11) Rashid, H.; Yaqub, G. Bioadsorbents and filters for removal of heavy metals in different environmental samples. *Nat. Environ. Pollut. Technol.* **2017**, 16, 1157–1164.

(12) Xiao, J. L.; Lv, W. Y.; Song, Y. H.; Zheng, Q. Graphene/nanofiber aerogels: performance regulation towards multiple applications in dye adsorption and oil/water separation. *Chem. Eng. J.* **2018**, 338, 202–210.

(13) Liu, Y.; Shi, T. H.; Zhang, T.; Yuan, D. S.; Peng, Y. X.; Qiu, F. X. Cellulose-derived multifunctional nano-CuO/carbon aerogel composites as a highly efficient oil absorbent. *Cellulose* **2019**, 26, 5381–5394.

(14) Pollanen, J.; Li, J. I. A.; Collett, C. A.; Gannon, W. J.; Halperin, W. P.; Sauls, J. A. New chiral phases of superfluid ^{3}He stabilized by anisotropic silica aerogel. *Nat. Phys.* **2012**, 8, 317–320.

(15) Mu, R. J.; Pang, J.; Yuan, Y.; Tan, X. D.; Wang, M.; Chen, H.; Chiang, W. Y. Progress on the structures and functions of aerogels. *Chin. J. Struct. Chem.* **2016**, 35, 487–497.

(16) Cesar, M. C. F.; Telma, M.; Durães, L.; Artur, J. M. V. Efficient simultaneous removal of petroleum hydrocarbon pollutants by a hydrophobic silica aerogel-like material. *Colloid. Surface. A* **2017**, 520, 550–560.

(17) Robitzer, M.; Tourrette, A.; Horga, R. Nitrogen sorption as a tool for the characterisation of polysaccharide aerogels. *Carbohyd. Polym.* **2011**, 85, 44–53.

(18) Chen, H.; Mu, R. J.; Pang, J.; Tan, X. D.; Wang, M. Structure and potential application of konjac glucomannan nano microfibril aerogel. *Chin. J. Struct. Chem.* **2016**, 35, 1942–1946.

(19) Zhang, Y.; Yang, J. C. E.; Fu, M. L.; Yuan, B. L.; Gupta, K. One-step fabrication of recycled Ag nanoparticles/graphene aerogel with high mechanical property for disinfection and catalytic reduction of 4-nitrophonel. *Environ. Technol.* **2019**, 40, 3381–3391.

(20) Chen, X.; Fang, D. Y.; Luo, X. L.; Wang, X. S.; Tong, C. L.; Pang, J.; Yan, Z. M.; Zheng, Y. F. Preparation, structures and mechanical properties of bamboo shoot shell nanofiber/konjac glucomannan aerogels. *Chin. J. Struct. Chem.* **2017**, 36, 2051–2057.

(21) Wang, J.; Zhao, D.; Shang, K.; Wang, Y. T.; Ye, D. D.; Kang, A. H.; Liao, W.; Wang, Y. Z. Ultrasoft gelatin aerogels for oil contaminant removal. *J. Mater. Chem. A* **2016**, 4, 9381–9389.

(22) Long, T.; Xu, Y.; Lv, X. J.; Ran, J. W.; Yang, S. B.; Xu, L. Y. Fabrication of the annular photocatalytic reactor using large-sized freestanding titania-silica monolithic aerogel as the catalyst for degradation of glyphosate. *Mater. Design* **2018**, 159, 195–200.

(23) Zhang, Y. S.; Khademhosseini, A. Advances in engineering hydrogels. *Science* **2017**, 356, eaaf3627.

(24) Chen, H.; Mu, R. J.; Pang, J.; Tan, X. D.; Lin, H. B.; Ma, Z.; Chiang, W. Y. Influence of topology structure on the stability of konjac glucomannan nano gel microfibril. *Chin. J. Struct. Chem.* **2015**, 34, 1939–1941.

(25) Xu, P.; Yao, Q.; Yu, N.; Zhou, Y.; Zhao, F.; Wang, B.; Peng, Z.; Hu, Z. Narrow-dispersed konjac glucomannan nanospheres with high moisture adsorption and desorption ability by inverse emulsion crosslinking. *Mater. Lett.* **2014**, 137, 59–61.

(26) Mu, R. J.; Yuan, Y.; Wang, L.; Ni, Y.; Li, M.; Chen, H.; Pang, J. Microencapsulation of lactobacillus acidophilus with konjac glucomannan hydrogel. *Food Hydrocolloid.* **2018**, 76, 42–48.

(27) Li, B.; Wang, Y. H.; Cheng, Y. J.; Ma, X. Y.; Pan, D. M.; Lin, Z. Surface changes of ochrobactrum anthropi in Cr(VI) treatment for I hour. *Chin. J. Struct. Chem.* **2009**, 2, 245–249.

(28) Wang, S.; Ning, H. M.; Hu, N.; Huang, K. Y.; Weng, S. Y.; Wu, X. P.; Wu, L. K.; Liu, J.; Alamusi. Preparation and characterization of graphene oxide/silk fibroin hybrid aerogel for dye and heavy metal adsorption. *Compos. Part B-Eng.* **2019**, 163, 716–722.

(29) Zhao, X.; Li, W.; Zhang, S. S.; Liu, L. H.; Liu, S. X. Hierarchically tunable porous carbon spheres derived from larch sawdust and application for efficiently removing Cr(III) and Pb(II). *Mater. Chem. Phys.* **2015**, 155, 52–58.

(30) Li, K. Q.; Zhou, Y.; Li, J.; Liu, J. M. Soft-templating synthesis of partially graphitic Fe-embedded ordered mesoporous carbon with rich micropores from bayberry kernel and its adsorption for Pb(II) and Cr(III). *J. Taiwan Inst. Chem. E.* **2018**, 82, 312–321.

(31) Žilić, S.; Mogol, B. A.; Akillioğlu, G.; Serpen, A.; Delić, N.; Gökmen, V. Effects of extrusion, infrared and microwave processing on maillard reaction products and phenolic compounds in soybean. *J. Sci. Food Agr.* **2014**, 94, 45–51.

(32) Liu, J. H.; Xu, Q. H.; Zhang, J. J.; Zhao, P. C.; Ding, Y. T. Characterization of silver carp (hypophthalmichthys molitrix) myosin protein glycated with konjac oligo-glucomannan. *Food Hydrocolloid.* **2016**, 57, 114–121.

(33) Luo, Y. Q.; Ling, Y. Z.; Wang, X. Y.; Han, Y.; Zeng, X. J.; Sun, R. C. Maillard reaction products from chitosan-xylan ionic liquid solution. *Carbohyd.*

Polym. **2013**, 98, 835–841.

(34) Liu, J.; Fang, C.; Xu, X.; Su, Q.; Zhao, P.; Ding, Y. Structural changes of silver carp myosin glycated with konjac oligo-glucomannan: effects of deacetylation. *Food Hydrocolloid.* **2019**, 91, 275–282.

(35) Shao, W. Y.; Liu, J. X.; Yang, K. G.; Liang, Y.; Weng, Y. J.; Li, S. W.; Liang, Z.; Zhang, L. H.; Zhang, Y. K. Hydrogen-bond interaction assisted branched copolymer HILIC material for separation and N-glycopeptides enrichment. *Talanta* **2016**, 158, 361–367.

(36) Wang, L.; Du, Y.; Yuan, Y.; Mu, R. J.; Gong, J. N.; Ni, Y. S.; Pang, J.; Wu, C. H. Mussel-inspired fabrication of konjac glucomannan/microcrystalline cellulose intelligent hydrogel with pH-responsive sustained release behavior. *Int. J. Biol. Macromol.* **2018**, 113, 285–293.

(37) Li, K.; Zhou, M.; Liang, L.; Jiang, L.; Wang, W. Ultrahigh-surface-area activated carbon aerogels derived from glucose for high-performance organic pollutants adsorption. *J. Colloid Interf. Sci.* **2019**, 546, 333–343.

(38) Liu, S. L.; Yao, F.; Olayinka, O.; Zhang, Z. H.; Fu, G. D. Green synthesis of oriented xanthan gum-graphene oxide hybrid aerogels for water purification. *Carbohyd. Polym.* **2017**, 174, 392–399.

(39) Zhang, T.; Xue, Y.; Li, Z. J.; Wang, Y. M.; Xue, C. H. Effects of deacetylation of konjac glucomannan on Alaska Pollock surimi gels subjected to high-temperature (120 degrees C) treatment. *Food Hydrocolloid.* **2015**, 43, 125–131.

(40) Tang, H. B.; Wang, L.; Li, Y. P.; Dong, S. Q. Effect of acidolysis and oxidation on structure and properties of konjac glucomannan. *Int. J. Biol. Macromol.* **2019**, 130, 378–387.

(41) Fan, S. S.; Tang, J.; Wang, Y.; Li, H.; Zhang, H.; Tang, J.; Wang, Z.; Li, X. D. Biochar prepared from co-pyrolysis of municipal sewage sludge and tea waste for the adsorption of methylene blue from aqueous solutions: kinetics, isotherm, thermodynamic and mechanism. *J. Mol. Liq.* **2016**, 220, 432–441.

(42) Araújo, C. S. T.; Almeida, I. L. S.; Rezende, H. C.; Marcionilio, S. M. L. O.; León, J. J. L.; Matos, T. N. D. Elucidation of mechanism involved in adsorption of Pb(II) onto lobeira fruit (solanum lycocarpum) using Langmuir, Freundlich and Temkin isotherms. *Microchem. J.* **2018**, 137, 348–354.

(43) Hu, Q. H.; Xiao, Z. J.; Xiong, X. M.; Zhou, G. M.; Guan, X. H. Predicting heavy metals' adsorption edges and adsorption isotherms on MnO_2 with the parameters determined from Langmuir kinetics. *J. Environ. Sci.* **2015**, 27, 207–216.

(44) Ge, K.; Yu, Q.; Chen, S.; Shi, X.; Wang, J. Modeling CO_2 adsorption dynamics within solid amine sorbent based on the fundamental diffusion-reaction processes. *Chem. Eng. J.* **2019**, 364, 328–339.